2020 IEEE/RSJ International Conference on Intelligent Robots and Systems (IROS)
October 25-29, 2020, Las Vegas, NV, USA (Virtual)

Microdrone-Equipped Mobile Crawler Robot System, DIR-3, for High-Step Climbing and High-Place Inspection

Yuji OGUSU, Kohji TOMITA, *Member, IEEE*, and Akiya KAMIMURA, *Member, IEEE*

***Abstract*— Mobile robots of various types have been proposed for infrastructure inspection and disaster investigation. For such mobile robot applications, accessing the areas is of primary importance for missions. Therefore, various locomotive mechanisms have been studied. We introduce a novel mobile robot system, named DIR-3, combining a crawler robot and a microdrone. By rotating its arm back and forth, DIR-3, a very simple, lightweight crawler robot with a single 360-degree rotatable U-shaped arm, can climb up/down an 18 cm high step, 1.5 times its height.**

Furthermore, to inspect high places, which is considered difficult for conventional mobile robots, a drone mooring system for mobile robots is presented. The tethered microdrone of DIR-3 can be controlled freely as a flying camera by switching operating modes on the graphic user interface. The drone mooring system has a unique tension-controlled winding mechanism that enables stable landing on DIR-3 from any location in the air, in addition to measurement and estimation of relative positions of the drone. We evaluated the landing capability, position estimation accuracy, and following control of the drone using the winding mechanism. Results show the feasibility of the proposed system for inspection of cracks in a 5 m high concrete wall.

I. Introduction

The Great East Japan Earthquake of 2011 and frequent disasters caused by the aging of various infrastructure facilities constructed during Japan's high-speed economic growth have increased the momentum for using robots in disaster surveys and infrastructure inspections. Specifically, robots are anticipated for use in searching for victims in collapsed houses and buildings or in checking for cracks on concrete walls that are at risk of collapse, as well as gas and raw material leaks, which pose a risk of fire or explosion to infrastructure facilities. Ideally, such an investigation robot must have capabilities for step-climbing, entering narrow spaces, and investigating high places.

To date, various land robots have been developed to improve stepping over capability: robots with flipper arms [1–6], folding arms [3, 7], link structures [8–10], and jump mechanisms [11, 12]. However, such robots traveling on the ground are usually too large and heavy to enter narrow spaces. Moreover, they have difficulty surveying higher places. On the other hand, inspection robots specializing in approaching narrow spaces have been studied. A typical robot is a snake-like robot [13–16] that can investigate narrow spaces such as the interior of pipes. Such a snake type robot, as well as land robots, has limitations in the heights it can reach. In many situations, it is necessary to conduct surveys of high places in disaster areas or infrastructure facilities. For this reason, robots that can access higher places have been studied. High-altitude surveys in outdoor environments are conducted actively using drones [17–19] recently, but it is challenging to apply drones to narrow spaces.

Y. Ogusu, K. Tomita, and A. Kamimura are with the National Institute of Advanced Industrial Science and Technology (AIST), Ibaraki 305-8568, Japan (e-mail: yuji.ogusu@aist.go.jp; k.tomita@aist.go.jp; kamimura.a@aist.go.jp).

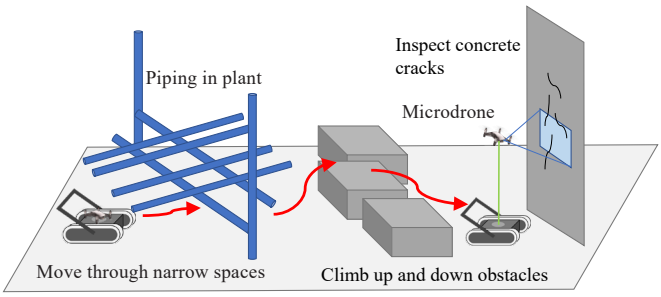

Figure 1. Application image of a microdrone-equipped mobile robot.

To the present day, robots with excellent step-climbing ability, narrow-area entry performance, and high-place inspection performance have been developed. In most cases, one capability might be superior to that of any other robot. As described herein, we present a practical small robot that excels in all areas of step-climbing, moving in narrow areas, and access to high places to support broader investigation both vertically and horizontally, as presented in Fig. 1. We present this novel mobile robot system combining a crawler robot and a microdrone. The microdrone mooring system is implemented on the mobile inspection robot, the Dexterous Inspection Robot (DIR-3), which is a small crawler robot with a single U-shaped arm used for high-step climbing.

The following are major contributions of this study.

- The compact crawler robot system having a single U-shaped arm that can climb high steps up to 1.5 times its height.
- The microdrone mooring system for mobile robots, which has a unique tension control winding mechanism that enables stable landing of the drone on the mobile robot and relative position measurement.
- Cracks on a 5 m high concrete wall can be inspected using the proposed system.

The remainder of the paper is organized as follows. Section II introduces the microdrone-equipped DIR-3 system. Section III describes and evaluates the microdrone relative position estimation. Section IV explains hardware experiments for real applications using the DIR-3 system, such as landing tests, following control of the drone, and inspection of cracks in high places. Finally, we conclude the paper and describe subjects of future work in Section V.

II. MICRODRONE-EQUIPPED DIR-3 SYSTEM

This section introduces the DIR-3 base crawler robot platform mechanical structures and control systems, and the microdrone mooring system.

A. *DIR-3 platform*

We have been developing crawler-type mobile robots [9, 10] able to climb higher steps than their own heights. The appearance of DIR-3 and its inner structure are presented in Fig. 2. Specifications of DIR-3 are presented in Table I.

The DIR-3 remote-controlled compact crawler robot, which is only 7.5 kg including a battery, is 37 cm long, 29 cm wide, and 12 cm high. The robot can enter height-limited narrow spaces with minimum 13 cm height and 30 cm width. The DIR-3 comprises two crawler tracks for locomotion on rough terrain, one U-shaped arm for step climbing/down, with looking upward/downward as portrayed in Fig. 4, and sensors presented in Fig. 2. DIR-3 can be operated with a game controller. The interface software provides a real-time camera image, robot posture, moving direction, and sensor information, as depicted in Fig. 3.

Conventional crawler robots use two or four flipper arms for step climbing [1–6]. However, as shown in Figs. 2 and 4, DIR-3 has only a single U-shaped arm enabling it to climb high steps automatically up to 18 cm: 1.5 times its height. The

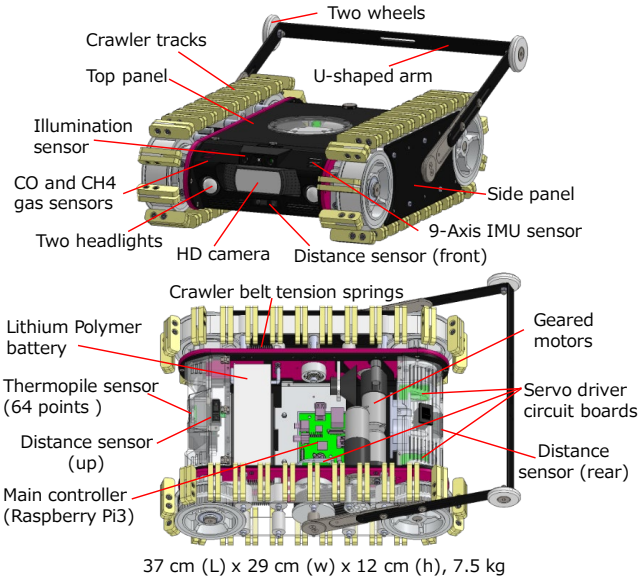

Figure 2. Appearance and inner structure of DIR-3 platform.

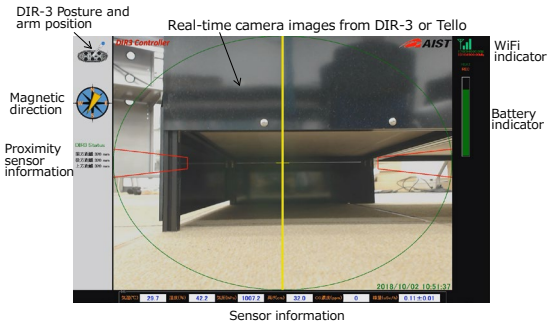

Figure 3. DIR-3 GUI system.

TABLE I
DIR-3 PLATFORM SPECIFICATIONS

Item	Value
Size	37 cm (L) × 29 cm (W) × 12 cm (H)
Weight	7.5 kg (including a battery)
Moving method, Max. speed	Crawler tracks, Max. 2 km/h
Gradeability	Max. 20 degrees (depending on ramp friction)
Actuators	Three Maxon motors with gear heads (RE-max 29, 0.9 Nm (24 VDC) for crawlers and RE-max 29, 18.5 Nm (24 VDC) for arm)
Servo drivers	Three original servo driver boards by AIST. Position and velocity control by commands via RS485 serial communication are supported
CPUs	Raspberry Pi 3 as main-controller board and Atmel ATmega168 on each servomotor driver
Internal communication	RS485 multi-drop connection (115.2 kbps)
RF communications	2.4 GHz WiFi for drone and 5 GHz WiFi for PC (Covered 100 m wide area in visible site)
Battery	Li-Po batteries (22.2 V 5.0 Ah)
Operation time	3 hr (depending on discharge rate)
Interface	Interface software on PC with a game controller

Figure 4. Usage of the U-shaped arm for climbing up an obstacle and inspecting upward/downward. The U-shaped arm can be rotated with 360 degrees about the axis so that posture recovery can be achieved when the robot turned over.

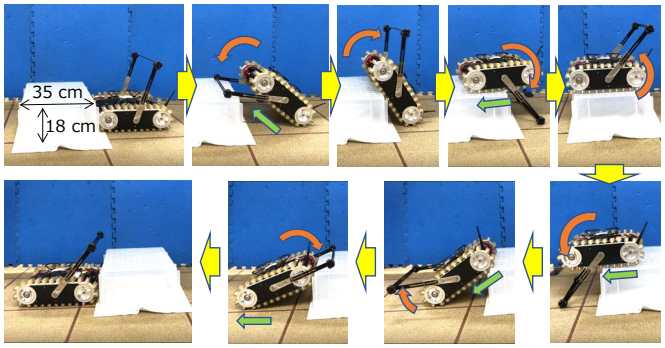

Figure 5. Step-climbing up and down motions. Orange and green arrows respectively show motions of rotating arm and crawler locomotion.

climbable height depends on the arm length, which is 28.8 cm currently. The arm is also used for posture recovery when the robot is turned over. The U-shaped arm can be rotated 360 degrees back and forth about the axes. Fig. 4 shows that the torque of rotation is sufficient to lift the front or back of the DIR-3 body. Two omni-wheels attached to the top of the U-shaped arm enable the robot to move smoothly in that configuration. Fig. 5 presents sequences of climbing up/down motions, which are achieved by timing control that is initiated automatically according to sensor information such as a gravity direction and arm angle. By collaborating with the arm

rotation and crawler motions, DIR-3 can climb and down a high step automatically. The current algorithm was developed for flat surfaces, but the robot itself can climb obstacles on non-flat surfaces using manual control of the arm. Because of space limitations, control algorithm details are not provided here, but the motions are presented with the attached video.

B. Microdrone mooring system

For most mobile robots, inspecting higher places is a difficult task because the robot is designed to move over the ground. A study by Miki et al. [20] examined a means by which a drone is used to make the small crawler robot climb a cliff that is difficult to climb on its own. They proposed a method to transport a tether mounted on a crawler robot by a drone, attach the tether to the top of the cliff, and then pull the tether to ascend the cliff. In their study, the drone and the small crawler robot are operated separately, and the small crawler robot can climb the cliff only once using a drone since the robot has no ability to unhook the hook. Studies by Kiribayashi et al. [21, 22] have examined the remote operation of a construction machine for disaster investigation using a moored drone. According to their study, the remote control is supported by taking off the drone from the construction machine and providing the operator with visibility information that cannot be obtained by the construction machine alone. The device was intended for outdoor use: it has great difficulty moving through narrow spaces because it uses large construction equipment.

A drone mooring system combined with the mobile robot system is proposed herein. We adopted a recent microdrone, the Ryze Tello Drone, which is sufficiently small to be mounted in a small area of the top panel, 150 mm × 200 mm, as shown in Fig. 6. The Tello Drone is only 80 g, with width of less than 10 cm. Tello has very stable flight for its size. It is possible to control the drone remotely using the Tello API package [23] written in the Go Programming Language. We combined the DIR-3 platform system and the Tello control system and implemented them with the DIR-3 inner controller.

To operate the battery-limited Tello drone and DIR-3 together, we propose the following scheme. During normal operations, an operator controls the DIR-3 to move to the target area remotely, and releases the microdrone only when inspections in higher places are required. Then the operator lands the drone again to continue a mission. The most challenging aspect of the scenario is landing the drone stably at the same place on DIR-3. One might use image processing with a camera and a marker, but a difficulty exists by which the marker becomes smaller as the position of the drone becomes higher. To date, several multirobot localization methods have been proposed [24–27]. In one earlier report of the literature [24], the ultrasonic and vision-based relative measurement method using the multiple robot network was proposed, but the relative measurement method using infrared LEDs and vision can not be used under strong sunlight. Another report [25] describes a vision-plus IMU system for localization among multiple UAVs. In yet another system [26], a stereo-vision-based multi-robot 6D localization and mapping system was presented. However, those vision-based approaches only allow operation between robots over close visible distances. Another report [27] describes multi-robot localization method using three ultrawideband (UWB) sensors for a tag robot and a single UWB sensor for a target robot, but it seems difficult to apply indoor environments surrounded by concrete walls, where radio multipaths are expected to be numerous. In spite of progress from those earlier studies, difficulties persist with landing control of a drone to the designated place of the robot. To resolve the issue simply and mechanically, we propose a drone mooring system connecting a tether to the bottom of the drone and retrieving it when landing, as depicted in Fig. 6.

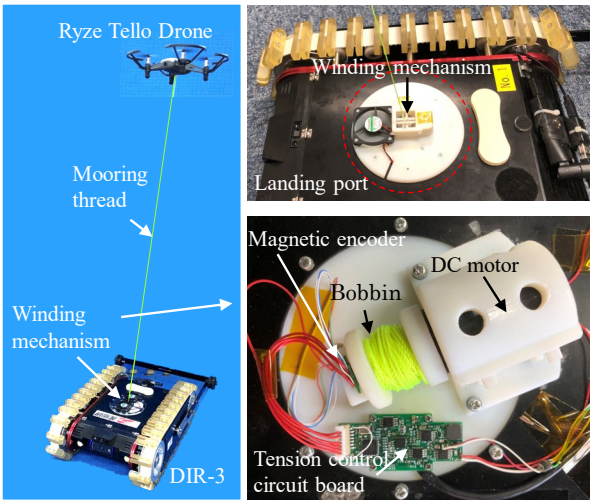

Figure 6. Microdrone mooring system. The developed winding mechanism is embedded under the center of the DIR-3 top plate.

The winding mechanism consists of a bobbin connected directly to a DC motor and a compact tension control circuit board that controls the motor torque by measuring the current to the motor. The circuit board keeps its winding tension constant to pull it softly to keep the thread rigid, at about 0.2 N, or to pull it forcefully, at about 1.13 N. During takeoff and during regular flight operation, the thread is pulled with 0.2 N. It is pulled with 1.13 N when landing and under normal crawler robot operations to attach the drone to the top panel of the DIR-3. The tension required for each situation was sought empirically with no disturbances such as wind. During takeoff and landing operations, the control command for the drone for each operation is sent first to the drone so that the drone executes the operations automatically. Then pulling control by the mechanism is activated. The left panel of Fig. 6 shows that the mooring thread is extended and appropriately stretched during flight operations. That is important to estimate the position of the drone hovering in the air. The maximum drone operating height is about 10 m currently.

C. Control system architecture of DIR-3

Fig. 7 presents control and communication systems among a host PC, DIR-3, and the microdrone. As the main controller for DIR-3 and Tello operations, Raspberry Pi 3 is installed inside the DIR-3 body. An extension I/O board is added on the Raspberry Pi board. Three original motor driver boards and the winding tension control board are connected to the I/O board with daisy-chain connection by RS485 serial communication and a power supply. Sensors such as nine-axis IMU and three proximity sensors are also connected to the extension I/O board.

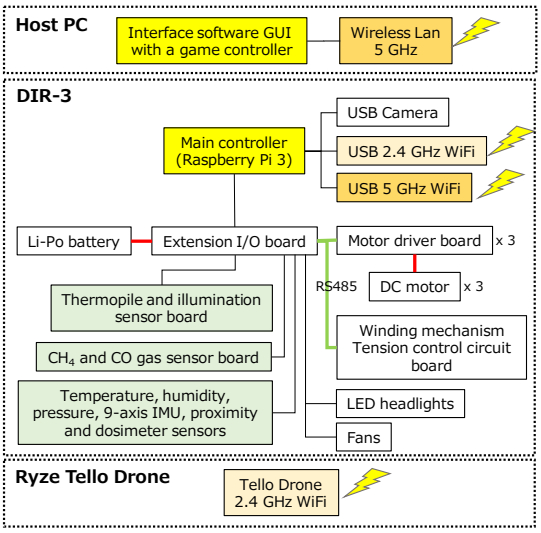

Figure 7. Control and communication systems of DIR-3.

Two WiFi communication channels are used for communication between DIR-3 and Tello drone (2.4 GHz) and for communication between the host PC and DIR-3 (5 GHz). In our WiFi communication system design, Tello drone operation is a subsystem of DIR-3. The operable distance of the drone is limited by the 5 GHz WiFi connection between DIR-3 and the host PC.

The interface software on the PC sends control commands to the DIR-3 main controller according to operation of the game controller. The Tello drone is also controlled by commands issued from the host PC by way of the DIR-3 main controller. Real-time camera images from DIR-3 and the Tello drone are transferred to the host PC via the DIR-3 main controller. Two control modes exist in the GUI system: DIR-3 and Tello operation modes. The operation modes are changed immediately by the game controller. The image on GUI and operations are changed accordingly. Drone operation by a user is simple: it is just like a flying camera. The GUI system is connected to the crack detection AI system on AWS via the internet. By sending an image to the cloud AI [28], a crack detection result image is returned with crack parts colored in red.

III. Microdrone Relative Position Estimation

This section presents an explanation of the relative position measurement mechanism and a position calculation method for a tethered drone. Ascertaining the relative positions of drone is useful and necessary for several applications such as high-place inspection and following control for the DIR-3.

A. Relative position measurement mechanism

We developed a compact relative position measurement mechanism suitable for use with mobile robot systems. The mechanism was combined with the winding mechanism as shown in Fig. 6. Fig. 8 presents the appearance and a sectional view of the relative position measurement mechanism. The mechanism comprises XY guide bars with XY gears that move freely in XY directions according to the thread pulling direction. The magnetic encoders placed below each XY gear measure rotation of gears and XY positions of the guide bars are calculated using the values. The magnetic encoder in Fig. 6 measures the bobbin rotation angle and the drawn length of the thread can be calculated accordingly.

The relative position of the drone (x, y, z) is calculated in centimeters using the thread drawn length d and XY guide bar positions (X, Y) in centimeters using Eq. (1).

$$\begin{cases} x = \frac{X}{h_X} \times \frac{d}{A} \\ y = \frac{Y}{h_Y} \times \frac{d}{A} \\ z = \frac{d}{A} + 15.0 \end{cases}, A = \sqrt{\frac{X^2}{h_X^2} + \frac{Y^2}{h_Y^2} + 1}, \quad (1)$$

Therein, h_X and h_Y respectively denote the heights of XY guide bars, as in Fig. 8 below: the values are 1.1 cm and 1.35 cm. The 15.0 cm in the equation for z represents the height from the ground with the drone landed on the back of the DIR-3. The measurable area by the mechanism in XY coordinate ranges [x_{min}, x_{max}] and [y_{min}, y_{max}] is determined by Eq. (2)

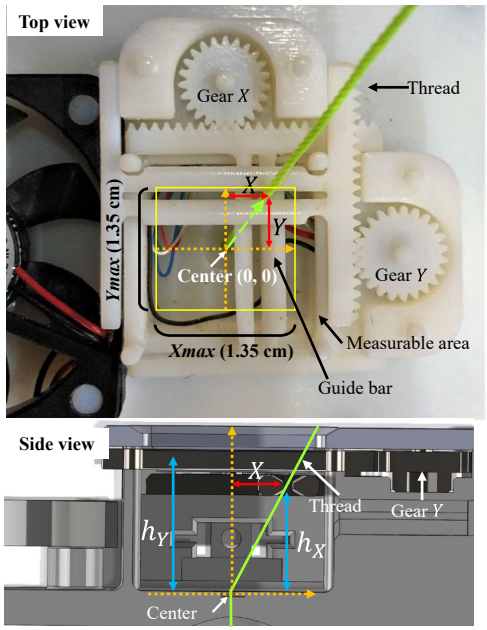

Figure 8. Relative position measurement mechanism.

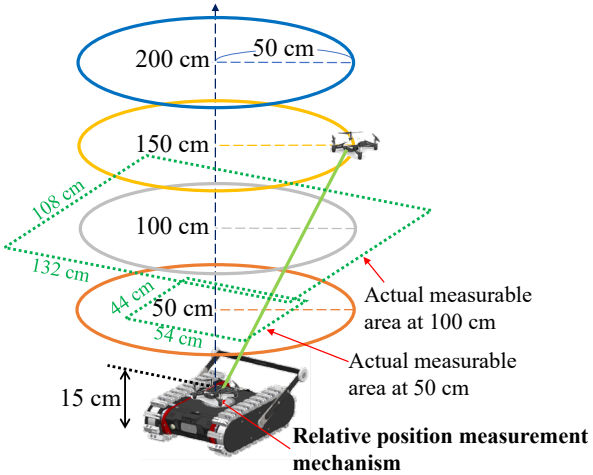

Figure 9. Relative position estimation experiment.

using d, height z, and the constant coefficients $\alpha = 0.5\, X_{max}/h_X \cong 0.7727$ and $\beta = 0.5\, Y_{max}/h_Y \cong 0.6296$.

$$\begin{cases} x_{max} = \alpha \cdot (z - 15.0) \\ x_{min} = -\alpha \cdot (z - 15.0) \\ y_{max} = \beta \cdot (z - 15.0) \\ y_{min} = -\beta \cdot (z - 15.0) \end{cases} \quad (2)$$

The measurable areas calculated using Eq. (2) have the shape of a reversed quadrangular pyramid because of the mechanism characteristics. For example, the green dotted line in Fig. 9 presents the actual measurable area at heights of 50 cm and 100 cm.

B. *Evaluation of drone relative position estimation*

We conducted hardware experiments shown in Fig. 9, to evaluate the feasibility of the proposed mechanism. We measured relative positions of the drone with heights of 50 cm, 100 cm, 150 cm, and 180 cm, with movement of the drone carefully along the circle with radius of 50 cm at each height. Figs. 10 and 11 respectively present relative position plots of each height in XY coordinates and XZ coordinates.

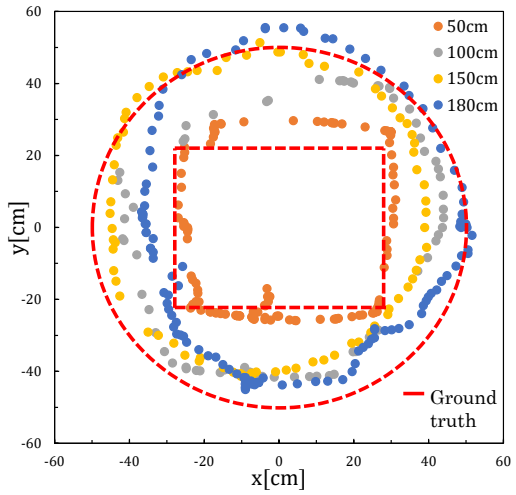

Figure 10. Relative position measurement results in XY coordinates.

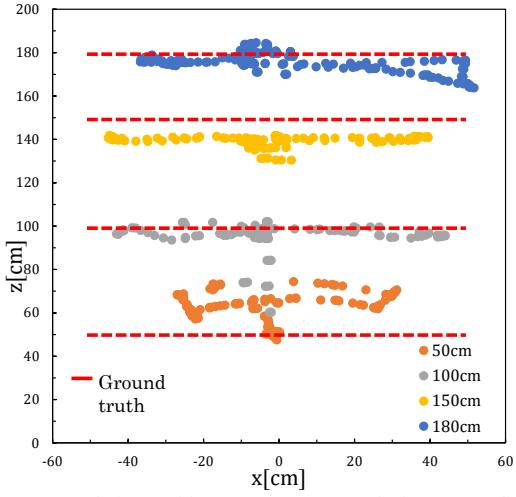

Figure 11. Relative position measurement results in XZ coordinates.

For the 50 cm height case, the drone trajectory was the rectangle with ranges [-27 cm, 31 cm] and [-26 cm, 30 cm] in XY coordinates. The calculated ranges by Eq. (2) in XY coordinates are [-27 cm, 27 cm] and [-22 cm, 22 cm]. The resulting rectangle size was found as 4 cm and 8 cm larger on the X and Y axes respectively than the calculated rectangle size at 50 cm height. This difference arises because a circle of 50 cm radius in Fig. 9 is larger than the measurable area at the 50 cm height by the mechanism. Errors of the estimated drone positions in the XY plane at heights of 100 cm, 150 cm, and 180 cm were less than about 15 cm as in Fig. 10. The average errors of height position estimation presented in Fig. 11 were, respectively from the bottom, about 13 cm, 5 cm, 8 cm, and 2 cm. The 13 cm error, on average, found for 50 cm height is attributable to the same reason found for the measurable area explained earlier. Experiment results showed that drone positions can be appropriately estimated at altitudes of 100 cm or more using the proposed mechanism. Of course, the position estimation error is expected to increase as the altitude increases, but it is applicable for following control at an altitude of about 1 m, as described in the next section.

IV. Hardware Experiments

We conducted hardware experiments to confirm the feasibility of the proposed microdrone-equipped crawler robot system.

A. *Examination of automatic landing by a mooring system*

Fig. 12 shows that we performed automatic landing tests using the winding mechanism with relative distance r and relative angle θ between the microdrone and the crawler robot of 1 m, 2 m, 90°, 60°, 45°, and 22.5°. Each test was performed five times and the success rates were calculated.

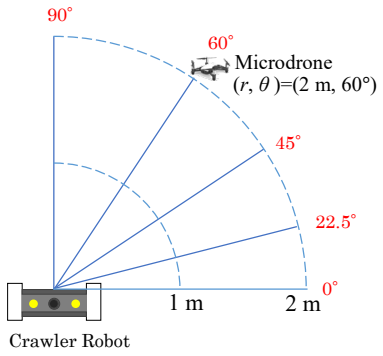

Figure 12. Experiment conditions for landing tests.

TABLE II
Results of Microdrone Landing Tests

Relative distance r	Relative angle θ	Success rate
1 m	90°	100%
1 m	60°	100%
1 m	45°	100%
1 m	22.5°	80%
2 m	90°	100%
2 m	60°	100%
2 m	45°	100%
2 m	22.5°	20%

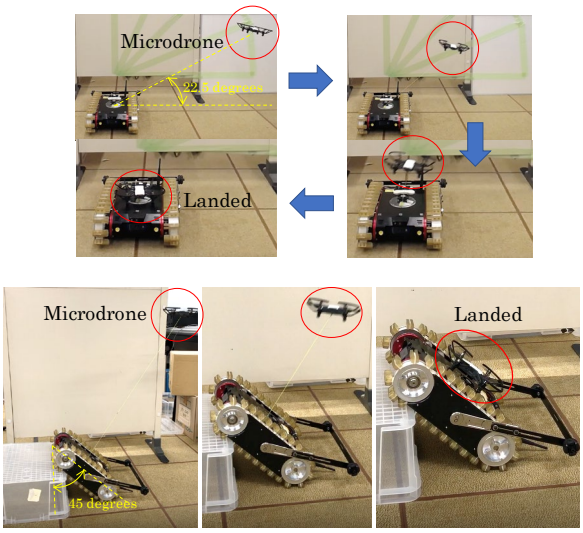

Figure 13. Microdrone landing tests.

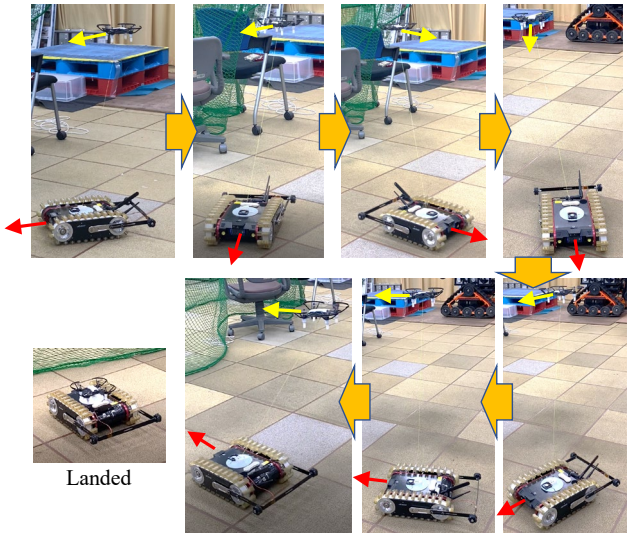

Figure 14. Following control experiment.

Table II presents a summary of the results. When the relative angle was greater than 45°, the landing success rate was 100% irrespective of the relative distance. However, in cases where the drone was at an angle of 22.5° or less, the drone contacted with the crawler track and the landing failed. Furthermore, as presented in Fig. 13, results demonstrated that the microdrone was able to land even when the crawler robot was inclined at 45°. The proposed winding mechanism demonstrated that the airborne microdrone at various positions can be landed stably on the top panel of the crawler robot irrespective of the crawler robot position and orientation.

B. *Following control experiments*

In DIR-3, because the crawler robot camera is mounted on the front panel at 6.5 cm above the ground, the visibility range is often narrow, making operation difficult. To overcome the shortcomings of the small robot with a narrow view range, we realized the following control by which the drone follows the crawler robot and provides a third-person view of the crawler robot. By applying following control with the drone when the view range becomes narrow, one can grasp the surrounding

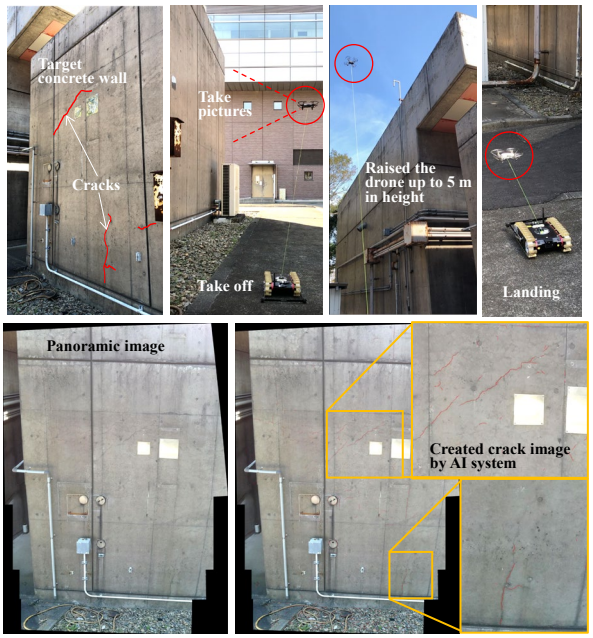

Figure 15. Higher place cracks inspection on a concrete wall by DIR-3. A panoramic image created from four taken pictures by the drone was sent to the crack detection AI system on AWS, and the crack detection image was generated.

situation easily. Therefore, improved operability can be expected. For the microdrone to follow the crawler robot, one must control both the relative position and the heading direction of the drone constant. The relative position is available using the mechanism proposed in section III. Relative azimuth between the microdrone and the crawler robot can be calculated using the value of magnetic compass installed on each. The relative position and the heading direction of the drone are controlled by the main controller of DIR-3 using P control with a 100 ms control period. We tested the following control of the drone as shown in Fig. 14. For the experiment, we moved the crawler robot while maintaining the drone hovering about 1 m directly above the center of the crawler robot. Results show that the microdrone is following as the crawler robot moves, as indicated by the yellow and red arrows in the figure.

C. *Inspection of high-place cracks on a concrete wall*

As presented in Fig. 15, we conducted an experiment for inspection of cracks high on a concrete wall. The crawler robot moved to the front of the concrete wall. Then the drone took off and flew vertically against the wall up to 5 m height.

For the experiment, we took four concrete wall images by the drone camera during the flight. The created panoramic image was sent to the AWS crack detection AI system [28] developed at AIST to generate a crack detection image. Currently, the AI system can detect cracks of 0.2 mm or greater width off-line. Detection method details were described in an earlier report [29].

Such concrete crack inspection has been achieved to date by human workers visually using high-cost scaffoldings. The results above showed the effectiveness of the proposed robotic system that can be used to inspect cracks at high places safely and inexpensively.

V. Conclusions and Future Work

We proposed a novel mobile robot system combining a small crawler robot, DIR-3, and a microdrone to realize an investigation robot that provides high-step climbing capability, a narrow approach, and inspection of higher places. We confirmed that the DIR-3 can climb up and down high steps automatically up to 1.5 times its height and can enter height-limited narrow spaces of 130 mm height and 300 mm width. We also developed a microdrone mooring system that enables both stable landings of the drone on the back of DIR-3 and relative position estimation of the drone for inspection of high places. Using the proposed relative position measurement mechanism, we realized following control of the drone and a third-person view for DIR-3 operation. Furthermore, we performed crack inspection of higher places on a 5 m high concrete wall and demonstrated the proposed system as useful and practical for inspection of high places.

As future research, to generate high-precision panoramic images, we plan to study a mechanism that captures images on the concrete wall automatically while measuring the drone position. Furthermore, power sharing between the drone and DIR-3 is a challenging issue that must be resolved.

Acknowledgment

We thank Dr. Takeshi Nagami in AIST who gave us valuable information for implementing an interface to the cloud AI system for crack detection.

References

[1] B. Yamauchi, "PackBot: A versatile platform for military robotics," *Proc. SPIE Unmanned Ground Vehicle Technology VI Conf.,* vol. 5422, 2004, pp. 228–237.

[2] J. A. Hesch, G. L. Mariottini, and S. I. Roumeliotis, "Descending-stair Detection, Approach, and Traversal with an Autonomous Tracked Vehicle," *Proc. IEEE/RSJ International Conference on Intelligent Robots and Systems*, 2010, pp. 5525–5531.

[3] B. Axelrod and W. H. Huang, "Autonomous door opening and traversal," *Proc. IEEE International Conference on Technologies for Practical Robot Applications (TePRA)*, 2015, pp. 1–6.

[4] iRobot 110 FirstLook, 2014. [Online]. Available: http://media.irobot.com/download/iRobot-110-FirstLook-Spec.pdf

[5] K. Nagatani, S. Kiribayashi, Y. Okada, S. Tadokoro, T. Nishimura, T. Yoshida, E. Koyanagi, and Y. Hada, "Redesign of rescue mobile robot Quince," *Proc. IEEE International Symposium on Safety, Security, and Rescue Robotics*, 2011, pp. 13–18.

[6] E. Rohmer, K. Ohno, T. Yoshida, K. Nagatani, E. Koyanagi, and S. Tadokoro, "Integration of a sub-crawlers' autonomous control in Quince highly mobile rescue robot," *Proc. IEEE/SICE International Symposium on System Integration*, 2019, pp. 78–83.

[7] K. Ueda, M. Guarnieri, R. Hodoshima, E. F. Fukushima, and S. Hirose, "Improvement of the remote operability for the arm-equipped tracked vehicle HELIOS IX," *Proc. IEEE/RSJ International Conference on Intelligent Robots and Systems*, 2010, pp. 363–369.

[8] H. Miyanaka, N. Wada, T. Kamegawa, N. Sato, S. Tsukui, H. Igarashi, and F. Matsuno, "Development of a unit type robot "KOHGA2" with stuck avoidance ability," *Proc. IEEE International Conference on Robotics and Automation*, 2007, pp. 3877–3882.

[9] A. Kamimura, "A Novel Mobile Robot Design for High Maneuverability," *Proc. IEEE/RSJ International Conference on Intelligent Robots and Systems*, 2006, pp. 4. (in Video proceedings)

[10] A. Kamimura and H. Kurokawa, "High-step climbing by a crawler robot DIR-2 - realization of automatic climbing motion -," *Proc. IEEE/RSJ International Conference on Intelligent Robots and Systems*, 2009, pp. 618–624.

[11] Boston Dynamics, "Leaps Small Buildings in a Single Bound-SandFlea," 2017. [Online]. Available: https://ozrobotics.com/leaps-small-buildings-single-bound-sandflea/

[12] S. Li and D. Rus, "JelloCube: A Continuously Jumping Robot With Soft Body," *IEEE/ASME Transactions on Mechatronics*, Vol. 24, Issue 2, 2019, pp. 447–458.

[13] T. Kamegawa, T. Yarnasaki, H. Igarashi et al., "Development of the snakelike rescue robot "kohga"," *IEEE International Conference on Robotics and Automation*, vol. 5, 2004, pp. 5081–5086.

[14] C. Wright, A. Buchan, B. Brown et al., "Design and architecture of the unified modular snake robot," *2012 IEEE International Conference on Robotics and Automation*, 2012, pp. 4347–4354.

[15] T. Kamegawa, W. Qi, H. Suhara et al., "Development of Tough Snake Robot in ImPACT Tough Robotics Challenge," *JSME Conference on Robotics and Mechatronics (Robomec)*, 2018, pp. 2A2–K05.

[16] M. Tanaka, M. Nakajima, and K. Tanaka, "Development of an Articulated Mobile Robot with Active Wheels and Manual Adaptation to Environment," *JSME Conference on Robotics and Mechatronics (Robomec)*, 2016, pp. 1A2–09a1.

[17] S. Adams, and C. Friedland, "A Survey of Unmanned Aerial Vehicle (UAV) Usage for Imagery Collection in Disaster Research and Management," *International Workshop on Remote Sensing for Disaster Response*, 15–16 September, 2011.

[18] B. E. Schäfer, D. Picchi, T. Engelhardt, and D. Abel, "Multicopter unmanned aerial vehicle for automated inspection of wind turbines," *2016 24th Mediterranean Conference on Control and Automation (MED)*, Athens, 2016, pp. 244–249.

[19] A. E. Jimenez-Cano, G. Heredia, and A. Ollero, "Aerial manipulator with a compliant arm for bridge inspection," *2017 International Conference on Unmanned Aircraft Systems (ICUAS)*, Miami, FL, USA, 2017, pp. 1217–1222.

[20] T. Miki, P. Khrapchenkov, and K. Hori, "UAV/UGV Autonomous Cooperation: UAV assists UGV to climb a cliff by attaching a tether," *2019 International Conference on Robotics and Automation (ICRA)*, 2019, pp. 8041–8047.

[21] S. Kiribayashi, K. Yakushigawa, and K. Nagatani, "Design and Development of Tether-Powered Multirotor Micro Unmanned Aerial Vehicle System for Remote-Controlled Construction Machine," *Conference on Field and Service Robotics*, 2017, pp. 637–648.

[22] S. Kiribayashi, K. Yakushigawa, and K. Nagatani, "Position Estimation of Tethered Micro Unmanned Aerial Vehicle by Observing the Slack Tether," *Safety, Security, and Rescue Robotics (SSRR)*, 2017, pp.159–165.

[23] The tello Go (golang) package, 2019. [Online]. Available: https://github.com/SMerrony/tello

[24] O. De Silva, G. K. I. Mann, and R. G. Gosine, "An ultrasonic and vision-based relative positioning sensor for multirobot localization," *IEEE Sens. J.,* vol. 15, no. 3, pp. 1716–1726, 2015.

[25] T. Nguyen, K. Mohta, C. J. Taylor, and V. Kumar, "Vision-based Multi-MAV Localization with Anonymous Relative Measurements Using Coupled Probabilistic Data Association Filter," *arXiv:1909.08200 [cs.RO]*, 2019.

[26] M. J. Schuster, K. Schmid, C. Brand, and M. Beetz, "Distributed stereo vision-based 6D localization and mapping for multi-robot teams," *J. F. Robot.,* vol. 36, no. 2, pp. 305–332, 2019.

[27] S. Güler, M. Abdelkader, and J. S. Shamma, "Infrastructure-free multi-robot localization with ultrawideband sensors," *Proc. the American Control Conference*, vol. 2019, pp. 13–18, 2019.

[28] Concrete Crack Detection Service (in Japanese), 2017. [Online]. Available: https://concrete.mihari.info/

[29] T. Kobayashi, "Spiral-Net with F1-Based Optimization for Image-Based Crack Detection," *Computer Vision – ACCV 2018*, Springer, vol. 11361, pp. 88–104, 2019.